Med Biol Eng Comput
DOI 10.1007/s11517-015-1271-1

ORIGINAL ARTICLE

Comparative study of a muscle stiffness sensor and electromyography and mechanomyography under fatigue conditions

Hyonyoung Han · Sungho Jo · Jung Kim

Received: 1 July 2013 / Accepted: 2 March 2015

Abstract This paper proposes the feasibility of a stiffness measurement for muscle contraction force estimation under muscle fatigue conditions. Bioelectric signals have been widely studied for the estimation of the contraction force for physical human–robot interactions, but the correlation between the biosignal and actual motion is decreased under fatigue conditions. Muscle stiffness could be a useful contraction force estimator under fatigue conditions because it measures the same physical quantity as the muscle contraction that generates the force. Electromyography (EMG), mechanomyography (MMG), and a piezoelectric resonance-based active muscle stiffness sensor were used to analyze the biceps brachii under isometric muscle fatigue conditions with reference force sensors at the end of the joint. Compared to EMG and MMG, the change in the stiffness signal was smaller ($p < 0.05$) in the invariable contraction force generation test until failure. In addition, in the various contraction level force generation tests, the stiffness signal under the fatigue condition changed <10 % ($p < 0.05$) compared with the signal under non-fatigue conditions. This result indicates that the muscle stiffness signal is less sensitive to muscle fatigue than other biosignals. This investigation provides insights into methods of monitoring and compensating for muscle fatigue.

H. Han · S. Jo (✉)
Department Computer Science, Korea Advanced Institute of Science and Technology, Daejeon, South Korea
e-mail: shjo@kaist.ac.kr

J. Kim (✉)
Department Mechanical Engineering, Korea Advanced Institute of Science and Technology, Daejeon, South Korea
e-mail: jungkim@kaist.ac.kr

Published online: 10 March 2015

Keywords Physical human–robot interaction (pHRI) · Muscle fatigue · Muscle stiffness sensor · Electromyography · Mechanomyography

1 Introduction

Motion estimation of human limbs can be applied to support the intuitive control of prostheses and to enhance physical strength. Fast motion intention recognition and robust motion information acquisition in various environmental conditions and estimation accuracy are required for natural limb motions during physical human–robot interactions (pHRIs) [1, 2]. As a biological actuator, skeletal muscle has a significant function in the control of force and motion in humans [3]. When humans intend any type of limb motion, the motor cortex in the brain activates and transmits the neural signals to the muscle fibers. Fibers that are stimulated by electrical impulses with an action potential contract and twitch. When the muscle fibers are activated, the components of muscle fiber (i.e., myosin and actin) pull each other so that the muscle shortens in the longitudinal direction and the components stack in the lateral direction, resulting in muscle thickening and enlargement of the muscle cross section. Concurrently, the physical properties of the bundle become dense and stiff. The combination of small fiber twitches also causes lateral oscillations. Bioelectric signals that measure physiological and physical changes in skeletal muscles provide motion intention recognition more rapidly than actual motion generation. Surface electromyography (EMG) measures the superimposed action potentials on the skin overlaying the muscles and is affected by the number of activated fibers and frequency of activation following the action potentials [4]; these action potentials are the inputs for the skeletal muscle, whereas the actual limb motions are the output signals of the muscle.

Mechanomyography (MMG) measures the lateral oscillations, which are related to the length, cross-sectional changes, and stimulation frequencies of the muscle fibers on the skin [5]. Therefore, skin properties such as skinfold thickness affect the vibrations [6]. Muscle stiffness is measured using an active muscle stiffness sensor (aMSS) [21] based on piezoelectric resonance [22–24]. This physical sensor can measure changes in stiffness through clothes, an important aspect of pHRIs. aMSS are also less sensitive than other sensors to skin conditions such as skin impedance (dry/wet) and skinfold thickness [21]. Studies of EMG, MMG, and aMSS have revealed that the features of the signals are highly correlated with the muscle contraction forces under general conditions. Therefore, it is possible to estimate the contraction force and, consequently, the joint torque, from the amplitudes acquired via EMG [7], MMG [8, 9], and aMSS.

However, the estimates gathered using EMG and MMG are distorted and exhibit time-varying behavior under muscle fatigue conditions. In physiology, muscle fatigue is usually defined as the loss of voluntary force-producing capacity during exercise [10, 11] and, more specifically, as a process that develops over time and progressively changes the characteristics of the material or the mechanism without an evident change in performance until the point of deformation or rupture [3]. The features of bioelectric signals over time have been analyzed in long-lasting sustained contraction tests under isometric conditions [12], and the signal features during repeated cycles of intermittent isometric contraction have been analyzed while subjects maintained a target amount of force [13]. During the generation of a constant force over a long period of time, the amplitude of the EMG signal increases, and its mean frequency decreases over time [14, 15]. The MMG signal amplitude decreases under fatigue [13, 16]. These studies demonstrate that muscle fatigue hinders the estimation of the contraction force. Some studies [17, 18] have investigated the inclusion of a compensating factor for this time-varying limitation in the estimation, but the problem remains challenging. From an engineering perspective, these limitations imply that biosignals cannot be fully employed as robust control inputs in pHRI devices.

The generated joint force can be intentionally and consistently maintained even under fatigue. Thus, the physical change in the muscle is more robust than the bioelectric signal, which is considered an control input for limb motion. Therefore, direct measurements of the physical changes in the muscle properties are expected to be resilient to muscle fatigue. This paper proposes the measurement of muscle stiffness [19, 20], which is a representative physical change in muscle during contractions. Stiffness is both a quantity that expresses a physical change in muscle activity and an intrinsic mechanical characteristic of a muscle.

This paper assesses muscle stiffness signals under muscle fatigue conditions. The time delays between the EMG and force signal [27] are known as electromechanical delays [25, 26], and the physical skeletal muscle intermediates between the neural signal and the actual motions. The aMSS measures the physical changes in the skeletal muscle, and the aMSS lies temporally between the EMG and force signal. Therefore, the aMSS signal should be resilient to muscle fatigue as a physical change in the muscle. The EMG and MMG signals were compared with aMSS; the features of each signal were extracted using temporal and spectral approaches. Long-lasting contractions and various contraction levels after fatigue were also examined. The signal features over time were analyzed statistically, and these results are discussed with respect to the physiological changes in the muscle.

2 Methods and materials

2.1 Muscle stiffness sensor

Generally, a mechanical body has a characteristic phenomenon called resonance: an object oscillates at a greater magnitude at a certain frequency. The properties of the resonance oscillations reportedly change when the oscillating body comes into contact with other mechanical bodies [28], and the resonance frequency of a material depends on its stiffness and its material density. As a material becomes stiffer, the resonance frequency increases, and the magnitude of the vibrations changes. Thus, it can be inferred that stiffness changes with changes in frequency. The stiffness can be measured by acquiring the magnitude of vibration which is a mechanical expression of the sensor's frequency response. Muscle stiffness is measured using an aMSS based on the correlation between stiffness and resonance.

The aMSS consists of a pair of resonating piezoelectric transducer (PZT) probes and a resonance signal processing circuit [21], as shown in Fig. 1a. In the PZT probe, the driving PZT generates a mechanical vibration, and the pickup PZT measures the vibration. To generate a continuous resonance in the resonance frequency of the probe ($f_r = 125$ kHz), the circuit creates the output signal, which is transmitted to the driving PZT, and the input signal, which is measured using the pickup PZT, identically at the resonance frequency using a band-pass filter ($f_{\text{cutoff}} = 100$–150 kHz), amplifier, and phase shifter. To measure the change in stiffness, two features are extracted from the resonance signal; Fig. 1a shows the conceptual relationship between the signals: S_f for resonance frequency and S_a for vibration amplitude detection. S_f can be extracted from a modified binary signal using a bias shifter and amplifier, and S_a can be acquired from a modified quasi-DC signal using an amplifier, rectifier, and low-pass filter to measure each feature without cross talk between the features. Figure 1b shows the correlation between each feature and contraction force under

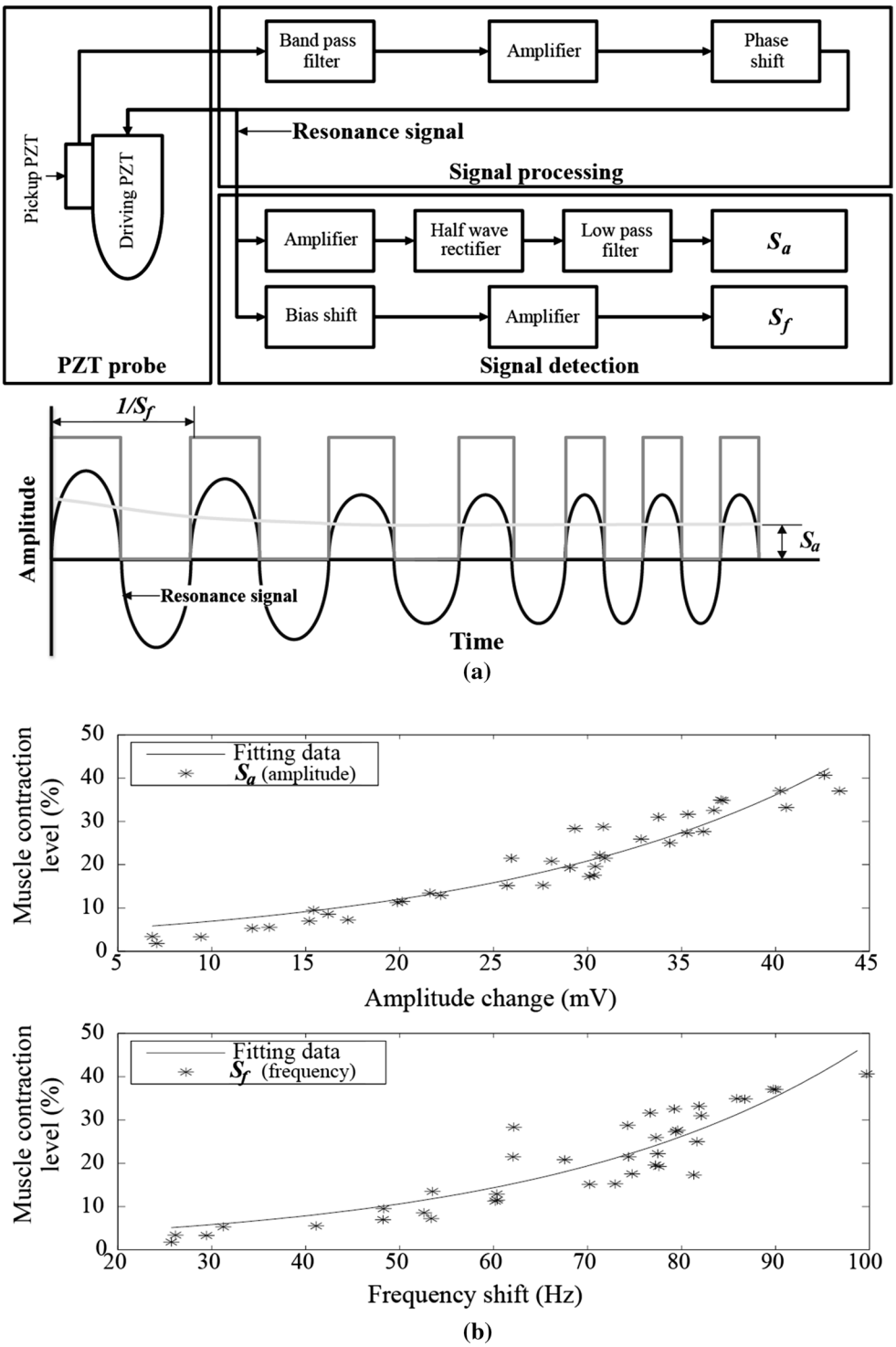

Fig. 1 **a** Composition of the aMSS: PZT probe, signal processing, and signal detection (*top*) correlation between signals; resonance signals S_f from frequency and S_a from amplitude (*bottom*). **b** Correlation between the muscle contraction level and aMSS signal [21]

isometric conditions. Each aMSS signal is exponentially correlated ($R > 0.9$) with the contraction force as depicted in Eq. (1), where F indicates the maximum voluntary contractions (MVCs) based on the muscle contraction level, S_x is each sensor signal (S_f and S_a), and A and B are constants.

$$F = A \times \exp(B \times S_X). \quad (1)$$

2.2 Subjects and experimental procedure

Twelve healthy subjects with no overt signs of neuromuscular disease volunteered to participate in the study and signed an informed consent form. The subjects comprised ten males and two females (average age 27.25 ± 3.86 years, average height 170.83 ± 9.78 cm,

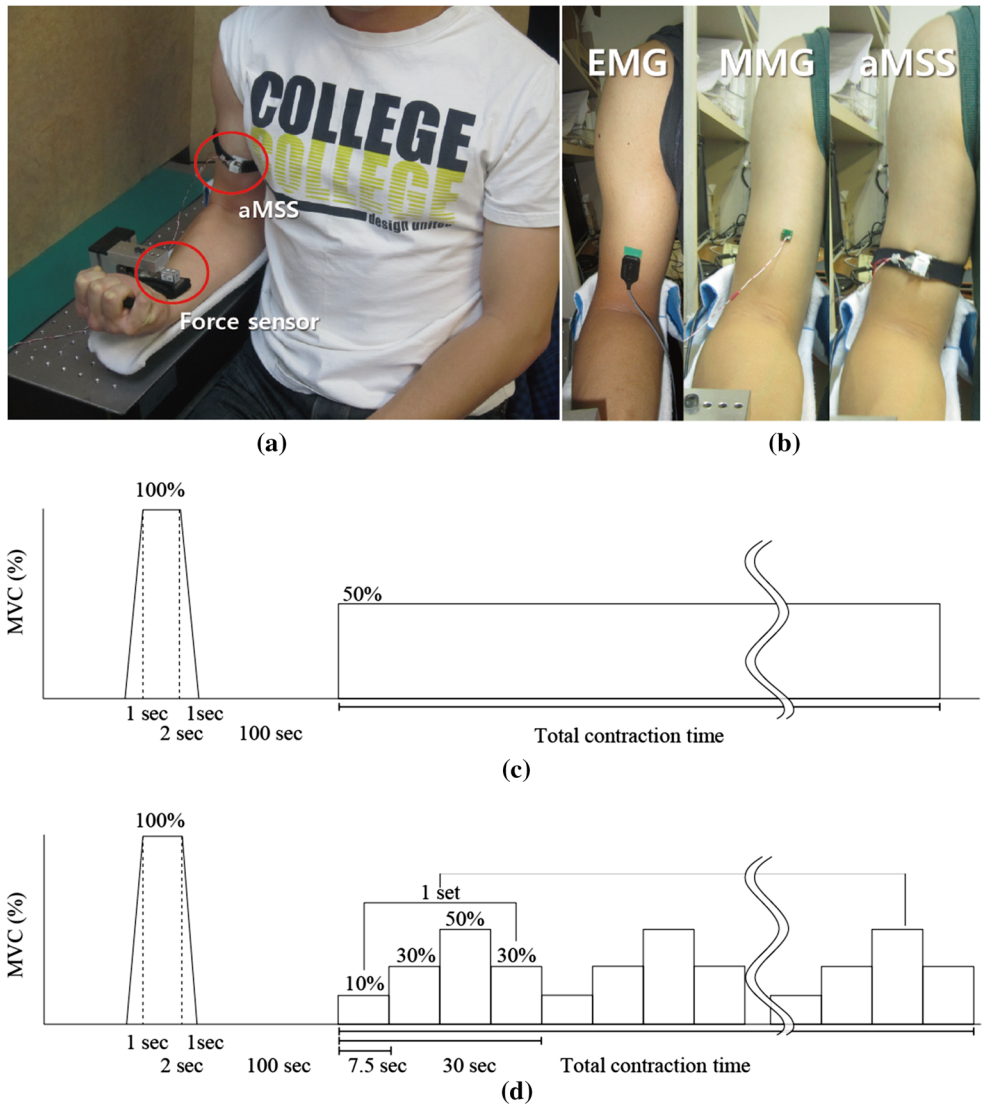

Fig. 2 Experimental setup and test protocols: **a** measurement sites for the force sensor and muscle contraction sensor (aMSS); **b** measurement sites for the sensors on the biceps brachii muscle; **c** test 1 under conditions of long-lasting contraction; **d** test 2 under conditions of varying contraction levels

average weight 68.25 ± 12.74 kg). This study was conducted according to the protocols approved by the Institutional Review Board of the Korea Advanced Institute of Science and Technology (KAIST).

The target motion was an isometric elbow flexion, and each signal was measured on the biceps brachii, which is the dominant agonist muscle for this motion. The upper arm and forearm were maintained vertically in a guide frame, as shown in Fig. 2a. The forearm was fixed using a cast frame that covered the area from the hand to the elbow, and the upper arm was guided separately using a vertical frame that only covered the back of the upper arm to avoid changes in the geometry of the muscle resulting from side covers. The force sensor was located at the end of the joint near the wrist and measured the elbow flexion force. Before the test, the individual MVC was measured using a force sensor. The subjects reached the maximal force by gradually increasing the force in 1-s increments and maintaining the force for 2 s for the MVC measurement. Then, the subjects rested for 100 s for muscle recovery before the main test. A program on the monitor in front of the subjects displayed the target and measured forces. The EMG, MMG, and aMSS signals were tested independently to acquire high-quality data at the optimal measurement site and to avoid cross talk between the sensors. The experiments were conducted in random order to reduce the order effect. Each sensor was attached near the belly center of the biceps brachii, which is the best sensor position for data acquisition,

as shown in Fig. 2b. To permit muscle recovery, the subjects rested for at least 6 h between tests.

Each sensor signal was assessed in two experiments: a long-lasting contraction at the unit level to compare sensors and continuously varying levels of change contractions to analyze individual sensors. In the first test, illustrated in Fig. 2c, the subjects were asked to maintain their elbow flexion at 50 % of their individual MVC following the guide program for as long as possible; the subjects tired when generating 50 % of their MVC [29]. For this experiment, the subjects were required to generate force until they could no longer sustain that level of force. Individual times differed, but all subjects generated force for longer than 60 s. The second test measured the signals for continuously varying levels of force contractions and is illustrated in Fig. 2d. One set consisted of four target forces (10, 30, 50, and 30 % MVC) in 7.5-s intervals (i.e., total duration = 30 s/set) until failure. Most subjects repeated the contraction set more than 10 times.

2.3 Measurement

The EMG, MMG, and aMSS signals were compared with the reference joint force signal. The EMG signals were measured using a commercial EMG system (Bagnoli-16; Delsys Inc, USA). The measured signals were conditioned by rejecting the power line noise (60 Hz) through a notch filter and band-pass filtering between 5 and 500 Hz through a fourth-order Butterworth filter. The MMG signals were measured using MEMS accelerometers (ADXL202JE; Analog Devices, Inc, USA), which are lightweight and small. The MMG signals were also processed to remove 60-Hz noise, and the desired information between the 5- and 150-Hz signals was extracted using the same filtering methods used for the EMG. The EMG and MMG signals, including the aMSS, were acquired using a 1-kHz sampling frequency with a 16-bit A/D converting board.

All sensor signals were analyzed based on both their temporal and spectral features. For aMSS, S_a and S_f were used directly as the temporal and spectral features. For EMG and MMG, the temporal feature was extracted using a mean absolute value (MAV) computation that indicates the smoothed amplitude waveform of the rectified raw signal as follows:

$$\mathrm{MAV} = \frac{1}{N}\sum_{k=1}^{N} |X_k|. \tag{2}$$

where N is the window length and x_k is the kth sample value of the raw signal. In this study, 200-ms windows ($N = 200$) were overlapped for smoothing. The time domain signals were transformed to the frequency domain using the fast Fourier transform (FFT) method with 250-ms windows. The mean frequency (MNF) was computed using Eq. (3) based on the FFT data, where k is the total number of frequency bins, I_k is the intensity of the spectrum at bin k, and f_k is the frequency of the spectrum at k:

$$\mathrm{MNF} = \frac{\sum_{k=0}^{N} I_k \cdot f_k}{\sum_{k=0}^{N} I_k}. \tag{3}$$

The EMG MNF and MMG MNF were determined only for comparison because the most commonly used signal for force estimation is the temporal domain signal.

Each feature trend was analyzed over time. The timescales of each signal were normalized with respect to the maximum time, which is the total contraction time, required to synchronize each different test time. Changes in the normalized features were analyzed statistically at every 20 % interval. The signals were normalized using a stable value within 5 s after initiation of the contractions. The change rates were analyzed based on these normalized values.

The subjects attempted to maintain constant contraction forces, but force fluctuations at values near the target force occurred due to the significant activation of the antagonist muscles and substantial changes in the direction of the net force of the activated muscles. Therefore, aspects of the signals should be compensated to analyze their features under constant force conditions. All sensor signals were divided by the force signal to compensate for fluctuations in the generated force, under the assumption that the sensor signals were proportional to the force in a small range. The force signals were then maintained at a constant value, and the other signals could be expected to be responses to the target force. The synchronization between the sensors was manually matched based on the activation onset time [30] of the reference force sensor, which was used in all tests.

2.4 Analysis methods

The test time of each subject differed significantly due to individual ability; thus, the signals were analyzed using the normalized test time. The total contraction time [31] was normalized by considering the activation start time as 0 and failure as 100 %. In the second test, the test set was analyzed using the same normalized test time. The signals were analyzed for every 20 % of normalized test time including the start time (i.e., 0, 20, 40, 60, 80, and 100 %).

The signal features were analyzed in two ways. First, the individual features were analyzed over time using a Bland–Altman plot [32], which is a graphical analysis method used to compare the performance of two sensor signals. The x axis is the average of each feature and the generated

force, and the y axis is the difference (as a percentage) between them. Therefore, the data were concentrated in the (1, 0) space under constant force conditions when a signal feature was highly correlated with the force.

Second, the features recorded during the last 5 s of the test were statistically analyzed using a Mann–Whitney U test, which is a nonparametric statistical hypothesis test used to assess whether each sample has independent trends. The Mann–Whitney U test compares the medians of independent samples under the null hypothesis that the medians of the two samples are identical. Consider two samples, sample A and sample B; this method counts the number of observations in sample B and sums the rank of the observed sample for each observation in sample A. The value of U reported in this analysis that is based on sample A (each signal features) is calculated as.

$$U_{\mathrm{A}} = N_{\mathrm{A}}N_{\mathrm{B}} + \frac{N_{\mathrm{A}}(N_{\mathrm{A}}+1)}{2} - \sum R_{\mathrm{A}} \tag{4}$$

where N_{A} is the number of features in A, N_{B} is the number of feature in B, and R_{A} is the observed ranks for feature A. This test also results in the approximated p value; therefore, we can indicate the difference between each feature based on p value.

3 Results

3.1 Feature changes in long-lasting isometric elbow flexion

For the fatigue conditions, subjects were required to generate 50 % MVC force until failure. Figure 3a illustrates one case of signal features. During the fatigue condition, the EMG MAV increased, and the EMG MNF and MMG MAV decreased gradually, in agreement with previous research. However, there were small changes in the aMSS S_a and aMSS S_f caused by the stiffness.

Figure 3b presents the statistical expressions for the feature changes in the sensor over the normalized times. The duration of the change depends on individual muscle performance. The amplitudes were also normalized using the initial amplitude to compare the change rates. The EMG MAV increased gradually during the middle of the trial and changed dramatically at the end of the trial. These results indicate that the subject could sustain the target force during the middle of the trial with little fatigue, after which point the subject felt strong fatigue. The EMG MNF decreased gradually. The MMG MAV decreased gradually at approximately the same rate from the beginning to the end of the trial, and the MMG MNF remained constant. A small increase in aMSS S_a was observed; the aMSS S_a signal increased initially and subsequently remained constant or exhibited a slight decrease, whereas the aMSS S_f signal behaved similar to aMSS S_a. The initial increase in the stiffness signal may be attributable to the damping property of the muscle and the contact problems stemming from the generated force. After stabilization, the stiffness signal, aMSS S_a and S_f, remained constant.

The features in Fig. 4a were analyzed using the graphical analysis method (Bland–Altman plot) described in Fig. 3. EMG(MAV)–force data are widely spread in the upper right quadrant. Both the average and difference of EMG(MAV)–force increased linearly during constant force exertion. This result indicates EMG(MAV) increases during the test. MMG(MAV)–force data were spread in the lower left quadrant. Both the average and difference of the MMG(MAV)–force data decreased linearly during the constant force exertion. This result indicates that MMG(MAV) decreased during the test. Both of the sensors indicate that there were communication errors between the sensors. However, the aMSS Sf–force data were concentrated in the center, and the ratio between the two signals was near zero (1, 0). The aMSS S_a–force data were similar to the aMSS S_f–force data but slightly lower. This finding indicates that there were few communication errors between the sensors and that the aMSS S_f and aMSS S_a reliably measured the muscle contraction during the long-term contraction test. The bias errors within the data may be attributable to the signal feature normalization process.

Each feature of the signals obtained from the subjects was statistically analyzed and is shown in Fig. 4b. The solid bars represent the averages of the features during the last 5-s signal of the test, and the error bars indicate individual standard deviations. The EMG MAV increased by 46.42 $\pm$ 29.13 % over its starting value, and the EMG MNF decreased by more than 6.79 $\pm$ 7.81 %. The MMG MAV decreased by 32 $\pm$ 25.27 %, whereas the MMG MNF increased by only 3.23 $\pm$ 14.11 %. The S_f increased by 11.50 $\pm$ 12.70 %, and the S_a increased by 23.83 $\pm$ 28.48 %. The trends of the EMG MAV and MMG MAV signals differed significantly at the 5 % significance level ($p < 0.05$) from the Mann–Whitney U test marked with asterisk. Thus, the MMG MNF, S_f, and S_a trends are similar to those of the force signal.

3.2 Feature changes in the varying contraction level test

Each signal feature was acquired under continuous activation-level change conditions, and each feature change was analyzed with respect to time. The signals from each subject were normalized over the maximum contraction time and amplitude to obtain the change trend for each signal feature. The individual standard deviations are represented as error bars on the graphs in the corresponding timescales. Figure 5a illustrates one case of feature changes in two sets according

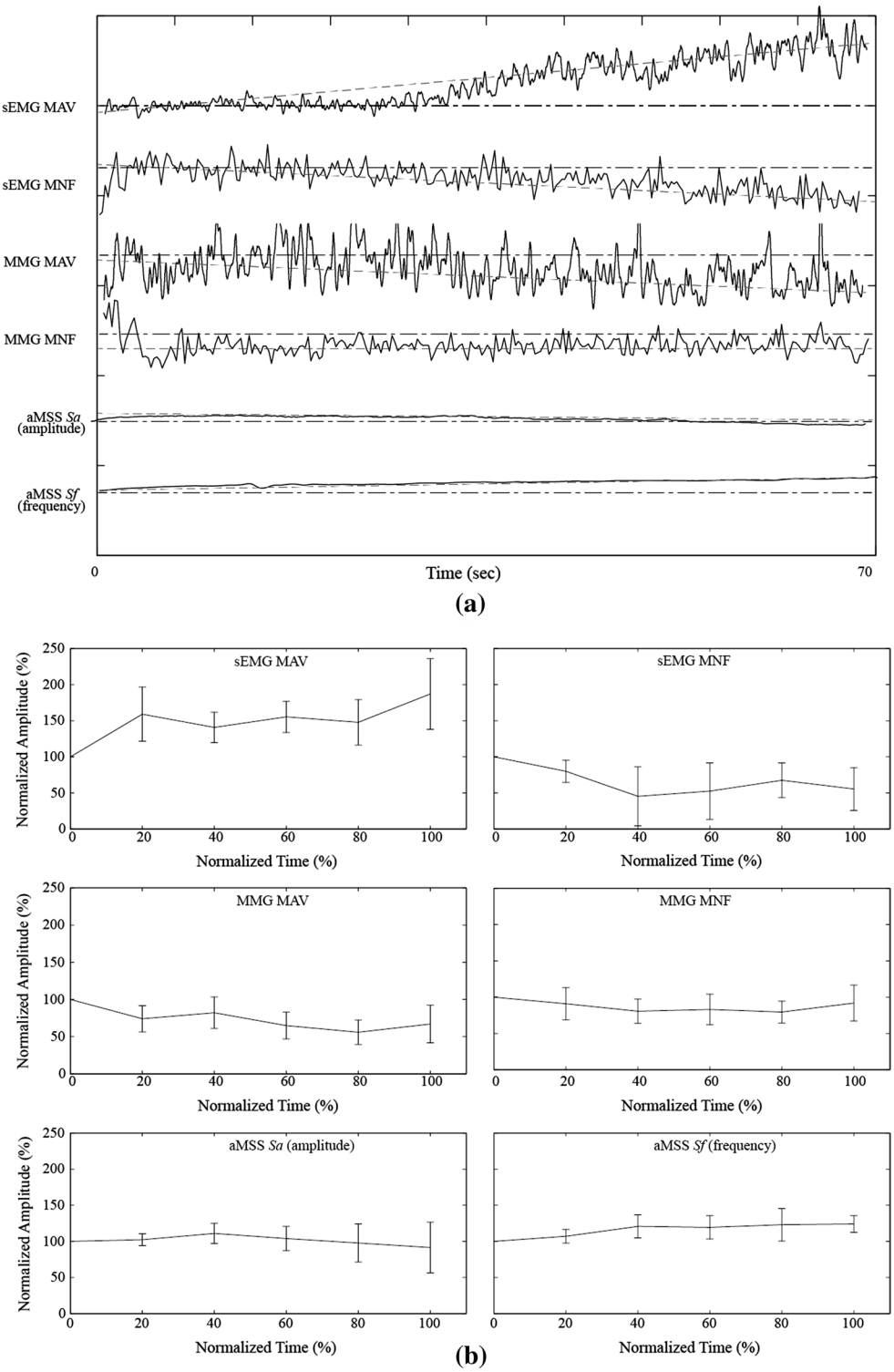

Fig. 3 **a** Feature changes in the EMG, MMG, and aMSS signals under fatigue conditions. The *dot-dash lines* indicate constant values, and the *dotted lines* indicate the fitting line for each signal. **b** Feature changes in the EMG, MMG, and aMSS normalized over time

to the time flow. Each level of activation according to the iteration sets is displayed in Fig. 5b. As the time increased, EMG MAV, EMG MNF, MMG MAV, and MMG MNF increased, even though the activation level was the same.

Each feature of the signal in the dynamic condition test described in Fig. 5 was analyzed statistically (Mann–Whitney *U* test). The graphs in Fig. 6 were grouped according to the activation level of each set (*X* axis), and data from the same level were plotted in time. Table 1 describes the correlation between time and activation-level changes in the groups in the same level during the dynamic condition test. This table presents the linear fitting

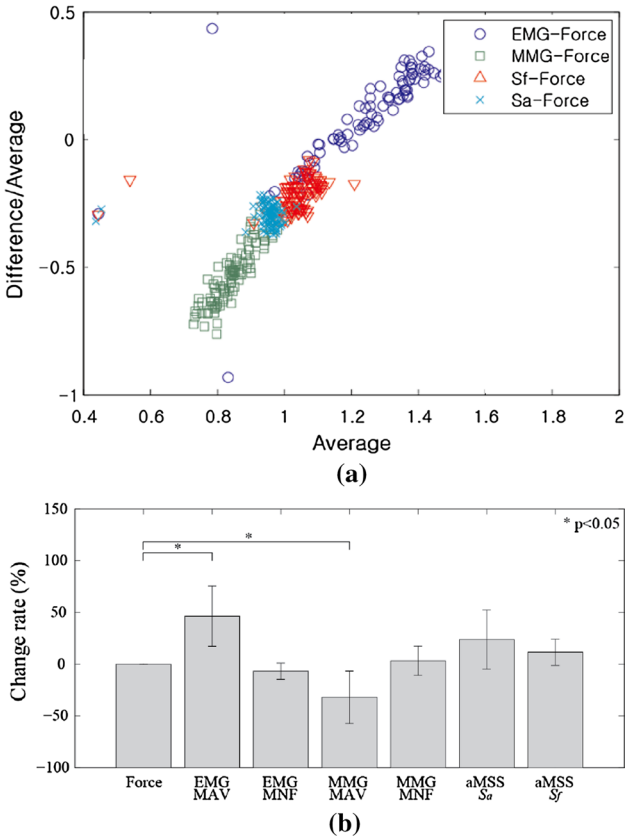

Fig. 4 **a** Bland–Altman plot of the signals under fatigue conditions. **b** Statistical analysis of each feature of the EMG, MMG, and aMSS signals compared with the muscle contraction force

coefficient in Eq. (5), in which Y, X, and R^2 are the sensor signal, normalized time, and correlation coefficient, respectively.

$$Y = \alpha X + \beta \tag{5}$$

In Fig. 7a, c, the EMG MAV and MMG MAV tend to increase significantly as time increases. There are few changes in the data and a low data change rate under 10 % MVC, but from 30 % MVC, there are significant changes ($p < 0.05$) in the data, and the data change rate increases with MVC level. Similar to the EMG MAV, the MMG MAV also increased. The data between each set in the 50 % MVC changed significantly, and the data change rates were the largest among the sensors. However, this result differs significantly from the results of the first test, indicating that the difference in the contraction type is due to static and dynamic contraction. The overall signal amplitude increased as the test set was repeated, which increased the fatigue, but the signal amplitude decreased at the subsequent same levels of target force. In Fig. 3a, the signal amplitude of the second set was larger than that of the first set, but the signal amplitude decreased significantly at the same level in the set, consistent with the observations of Yoshitake et al. [12] and Madeleine et al. [27]. The MMG MAV decreased in the long-lasting contraction tests [12] and increased in the dynamic contraction tests [27]. However, the MMG MNF did not change. Meanwhile, the aMSS S_a did not change significantly as time increased, as shown in Fig. 6e. Table 1 shows the activation-level change rate, which is α in Eq. (4), in the three cases. In agreement with the statistical analysis, aMSS S_a exhibited the lowest rate across the three conditioned force levels (MVC 10, 30, 50 %). For EMG MNF and MMG MNF, no significant change in aMSS S_f was observed over time, as shown in Fig. 6b, d, f. However, as shown in Table 1, aMSS S_f exhibited the lowest rate of change among all three measurements at all conditioned force levels.

4 Discussion

These results indicate that the force activation levels were estimated robustly under fatigue conditions using the stiffness signals and can be explained based on the physiological muscle contraction process. Figure 7 describes the contraction process in the right direction of the order. EMG signals are extracted before the muscle contraction from the neural signal, and the force is measured at the end of the sequence of interactions between the tendon and bone affecting the limb motion [4]. The mechanical property-based aMSS signal can be measured simultaneously with muscle contractions. The aMSS is sufficiently rapid to estimate motions, and its mechanical sensing is highly correlated with the generated joint force, even during long-term contractions. The MMG signal extracts the physical property-based information through the skin; thus, the MMG signal is affected by the properties of both the skin and muscle.

EMG signals are typically not directly proportional to the muscle contraction force due to the other component effects stated previously; however, under isometric conditions, this relationship can be considered linear [7]. This study examined isometric contraction conditions to evaluate only muscle property changes in the absence of other effects, such as the tendon force–length–velocity relationship. However, this linear relationship is disrupted under fatigue conditions. While the generated contraction force remains constant, the central nervous system attempts to compensate the power due to the temporarily reduced force production [10, 11]. Under fatigue conditions, the number of activated muscle fibers increases while the firing rate decreases. This indicates that the amplitude of the EMG signal increases while its MNF decreases and the amplitude of the MMG signal decreases [13]; however, the output, i.e., the joint force, remains constant. This could be interpreted as a change in the muscle fiber activation signal while the physical muscle bundle properties remain the same.

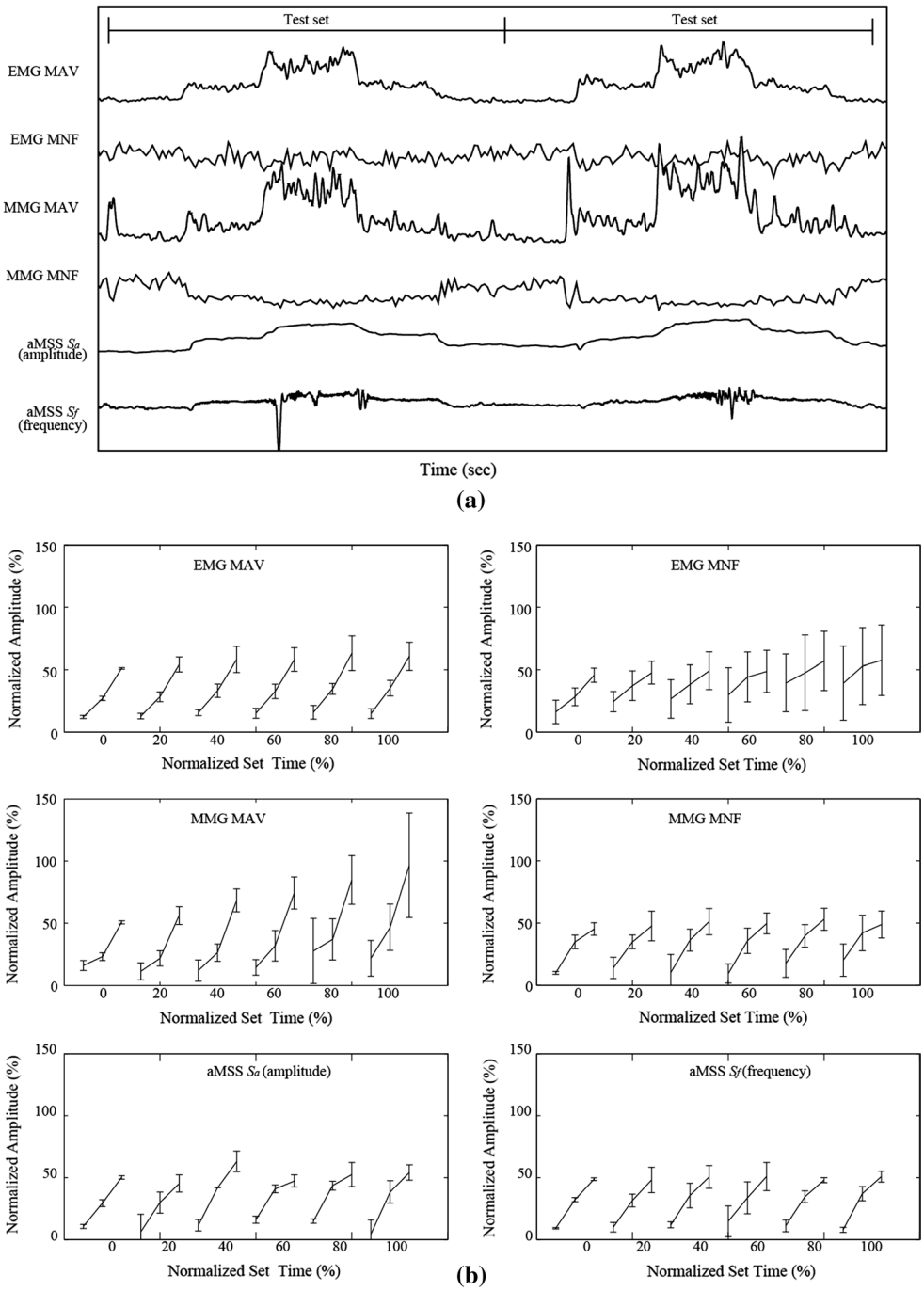

Fig. 5 **a** Feature changes in the EMG, MMG, and aMSS signals under dynamic fatigue conditions. **b** Feature changes in EMG MAV, EMG MNF, MMG MAV, MMG MNF, S_a (amplitude), and S_f (frequency) according to the iteration set. The three data points indicate activation levels of 10, 30, and 50 % from the *front line*

However, individual variables must be considered. The muscle stiffness measurements using an aMSS signal were analyzed using a previously developed mathematical model. The frequency shifts in the aMSS signal were expressed in accordance with Eq. (6) [21], and the amplitude changes in the sensor were expressed in accordance with Eq. (7).

$$s_f \approx \frac{1}{2\pi^2} \cdot \left(\frac{k_x}{Z_{\text{pzt}}}\right). \tag{6}$$

$$S_a \approx |C_1 - C_2 k_x|. \tag{7}$$

$$k_x = 2\left(\frac{S}{\pi}\right)^{1/2} \frac{Y}{(1-\upsilon^2)}. \tag{8}$$

In the mathematical model, k_x represents the effective muscle stiffness, Z_{PZT} represents the impedance of the PZT, and C_x represents constant variables. The effective stiffness (k_x)

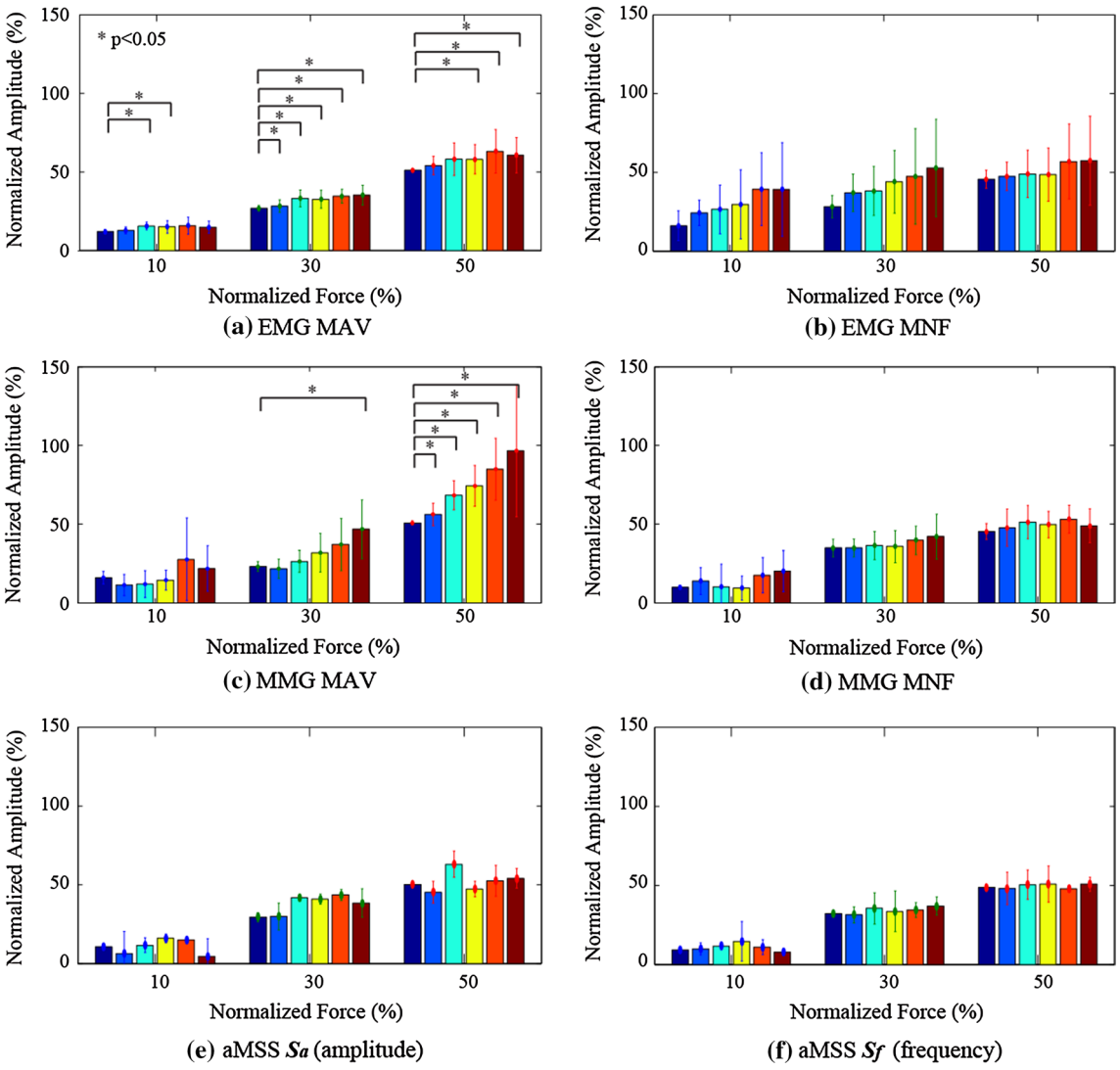

Fig. 6 Feature changes in the EMG, MMG, and aMSS between non-fatigue and fatigue conditions

Table 1 Data change rates according to activation level during fatigue. α and β are fitting coefficients in Eq. (5)

MVC (%)	EMG			MMG				aMSS		
	α	β	R^2	α	β	R^2		α	β	R^2
MAV										
10	0.63	12.09	0.58	2.68	9.58	0.36	*Sa* (amplitude)	0.01	10.59	0.25
30	1.72	25.75	0.88	4.61	15.03	0.80		1.23	33.95	0.89
50	2.14	50.00	0.84	8.92	38.21	0.94		0.23	46.59	0.35
MNF										
10	4.67	12.84	0.94	1.75	7.42	0.50	*Sf* (frequency)	0.01	15.26	0.70
30	4.56	25.32	0.97	1.43	32.24	0.82		0.73	32.69	0.74
50	2.47	42.21	0.84	0.94	45.00	0.41		0.38	46.62	0.85

is a function of the contact area (S), the material's Young's modulus (Y), and the Poisson ratio (ν), as described in Eq. (8). Therefore, changes in the signals are anticipated due to changes in the contact area resulting from muscle expansion and band elasticity. Increasing the contact area increases k_x, S_β, and S_a. Another aspect to consider is the thermal drift of

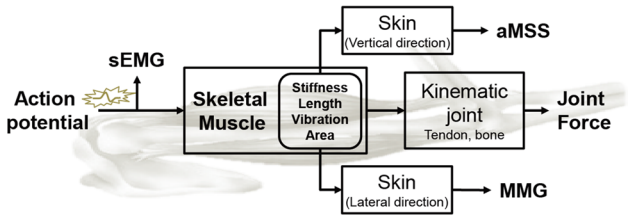

Fig. 7 Muscle activation and joint force generation process

the sensor, which is a characteristic of the PZT. After contact, the temperature of the PZT may increase with body temperature, inducing a thermal drift. The signal should compensate for this thermal effect. The maximum contraction forces, skinfold thickness, and skin tissue elasticity could also contribute to individual variances. Despite these limitations, our results demonstrate that the trends in the recorded signal are similar to those of the reference force signal.

5 Conclusion

This paper compares the performance of aMSS with that of EMG and MMG under muscle fatigue conditions. After the onset of fatigue, the measured EMG and MMG signals differ significantly from the previous patterns, although the same force from the force sensor is constantly applied. However, the aMSS, which measures a physical stiffness change in the muscle, is sufficiently resilient to muscle fatigue, which is one of the biggest challenges facing physical human–robot applications such as exoskeletons. A combination of biosignal sensors could improve the estimation of joint motion by reducing the limitations of each individual sensor. The development of a physiological and physical model for stiffness changes and corresponding limb motions that considers other mechanical properties and effects of tendons is also required. This study was conducted under isometric contraction conditions to analyze muscle properties accurately. In future research, the sensor will be tested under dynamic conditions for more practical pHRI applications.

Acknowledgments This research was supported by the Public welfare and Safety research program through the National Research Foundation of Korea (NRF) funded by the Ministry of Science, ICT and Future Planning (2010-0020449), and supported by the Ministry of Education under Basic Science Research Program through the National Research Foundation of Korea (2013R1A1A2009378).

References

1. Bien Z, Park K, Jung J, Do J (2005) Intention reading is essential in human-friendly interfaces for the elderly and the handicapped. IEEE Trans Ind Electron 52:1500–1505
2. Dellon B, Matsuoka Y (2007) Prosthetics, exoskeletons, and rehabilitation [Grand Challenges of Robotics]. IEEE Robot Autom Mag 14:30–34
3. Merletti R, Parker PA (2004) Electromyography: physiology, engineering, and noninvasive applications. Wiley-IEEE Press, New Jersy
4. Lieber R (2002) Skeletal muscle structure function and plasticity: the physiological basis of rehabilitation. Lippincott Williams & Wilkins, London
5. Orizio C, Perini R (1989) Veicsteinas A. Muscular sound and force relationship during isometric contraction in man. Eur J Appl Physiol Occup Physiol 58:528–533
6. Smith TG, Stokes MJ (1993) Technical aspects of acoustic myography (AMG) of human skeletal muscle: contact pressure and force/AMG relationships. J Neurosci Meth 47:85–92
7. Buchanan TS, Lloyd DG, Manal K, Besier TF (2004) Neuromusculoskeletal modeling: estimation of muscle forces and joint moments and movements from measurements of neural command. J Appl Biomech 20:367–395
8. Akataki K, Mita K, Watakabe M, Itoh K (2001) Mechanomyogram and force relationship during voluntary isometric ramp contractions of the biceps brachii muscle. Eur J Appl Physiol 84:19–25
9. Silva J, Heim W, Chau T (2005) A self-contained, mechanomyography-driven externally powered prosthesis. Arch Phys Med Rehab 86:2066–2070
10. Zwarts MJ, Bleijenberg G, Van Engelen BGM (2008) Clinical neurophysiology of fatigue. Clin Neurophysiol 119:2–10
11. Bigland-Ritchie B, Jones DA, Hosking GP, Edwards RH (1978) Central and peripheral fatigue in sustained maximum voluntary contractions of human quadriceps muscle. Clin Sci Mol Med 54:609–614
12. Yoshitake Y, Ue H, Miyazaki M, Moritani T (2001) Assessment of lower-back muscle fatigue using electromyography, mechanomyography, and near-infrared spectroscopy. Eur J Appl Physiol 84:174–179
13. Orizio C, Gobbo M, Diemont B, Esposito F, Veicsteinas A (2003) The surface mechanomyogram as a tool to describe the influence of fatigue on biceps brachii motor unit activation strategy. Historical basis and novel evidence. Eur J Appl Physiol 90:325–336
14. Viitasalo JHT, Komi PV (1977) Signal characteristics of EMG during fatigue. Eur J Appl Physiol Occup Physiol 37:111–121
15. Madeleine P, Jrgensen L, Sgaard K, Arendt-Nielsen L, Sjgaard G (2002) Development of muscle fatigue as assessed by electromyography and mechanomyography during continuous and intermittent low-force contractions: effects of the feedback mode. Eur J Appl Physiol 87:28–37
16. Beck TW, Housh TJ, Johnson GO, Weir JP, Cramer JT, Coburn JW, Malek MH (2004) Mechanomyographic amplitude and mean power frequency versus torque relationships during isokinetic and isometric muscle actions of the biceps brachii. J Electromyogr Kinesiol 14:555–564
17. Song JH, Jung JW, Bien Z (2006) Robust EMG pattern recognition to muscular fatigue effect for human-machine interaction. Lect Notes Artif Intell. 4293:1190–1199
18. Artemiadis PK, Kyriakopoulos KJ (2010) An EMG-based robot control scheme robust to time-varying EMG signal features. IEEE Trans Inf Technol Biomed 14:582–588
19. Murayama Y, Haruta M, Hatakeyama Shiina YT, Sakuma H, Takenoshita S, Omata S, Constantinou C (2008) Development of a new instrument for examination of stiffness in the breast using haptic sensor technology. Sens Actuators A 143(2):430–438
20. Arokoski J, Surakka J, Ojala T, Kolari P, Jurvelin JS (2005) Feasibility of the use of a novel soft tissue stiffness meter. Physiol Meas 26:215

21. Han H, Kim J (2013) Active muscle stiffness sensor based on piezoelectric resonance for muscle contraction estimation. Sens Actuators A Phys 194:212–219
22. Jalkanen V, Andersson BM, Bergh A, Ljungberg B, Lindahl OA (2008) Explanatory models for a tactile resonance sensor system elastic and density related variations of prostate tissue in vitro. Physiol Meas 29:729–745
23. Omata S, Terunuma Y (1992) New tactile sensor like the human hand and its applications. Sens Actuators A Phys 35:9–15
24. Omata S, Murayama Y, Constantinou CE (2004) Real time robotic tactile sensor system for the determination of the physical properties of biomaterials. Sens Actuators A Phys 112:278–285
25. Cavanagh PR, Komi PV (1979) Electromechanical delay in human skeletal muscle under concentric and eccentric contractions. Eur J Appl Physiol Occup Physiol 42:159–163
26. Norman RW, Komi PV (1979) Electromechanical delay in skeletal muscle under normal movement conditions. Acta Physiol Scand 106:241–248
27. Madeleine P, Bajaj P, Søqaard K, Arendt-Nielsen L (2001) Mechanomyography and electromyography force relationships during concentric, isometric and eccentric contractions. J Electromyogr Kinesiol 11(2):113–121
28. Krishna M, Rajanna K (2004) Tactile sensor based on piezoelectric resonance. IEEE Sens J 4(5):691–697
29. Borg G (1998) Borg's perceived exertion and pain scales. Human Kinetics, Champaign
30. Allison GT (2003) Trunk muscle onset detection technique for EMG signals with ECG artifact. J Electomyogr Kinesiol 13:209–216
31. Orizio C, Solomonow M, Baratta R, Veicsteinas A (1992) Influence of motor units recruitment and firing rate on the soundmyogram and EMG characteristics in cat gastrocnemius. J Electomyogr Kinesiol 2(4):232–241
32. Bland JM, Altman DG (1999) Measuring agreement in method comparison studies. Stat Methods Med Res 8:135–160